Design of Reactive Crystallization Systems Incorporating Kinetics and Mass-Transfer Effects

Vaibhav V. Kelkar and Ka M. Ng
Dept. of Chemical Engineering, University of Massachusetts, Amherst, MA 01003

A coherent approach for the design of reactive crystallization systems is presented by incorporating reaction and crystallization kinetics, and mass transfer, into an existing equilibrium-based conceptual design method. A generic model for a well-mixed crystallizer is developed; it is applicable to reacting systems with any number of components. The reaction, mass-transfer and dissolution Damköhler numbers, and the nucleation and growth numbers which result from the generic model, represent the relative rates of the individual steps, and their effect on the resulting crystal-size distribution and the crystallizer productivity is discussed. Estimates are provided for the typical values of the dimensionless numbers. To describe the solubility behavior of solid-liquid systems, a generalized equation for the isothermal solubility of a solute in the presence of an arbitrary number of other components is presented. The effects of the dimensionless numbers on the process paths are shown on the phase diagrams for systems involving up to four components. The utility of this integrated approach in the design of reactive crystallization systems is discussed using examples involving single and coprecipitation systems, and a salting out crystallization system.

Introduction

Reactive crystallization, or precipitation, involves reaction between reactants to form a solute which crystallizes into a solid product. Examples of industrial relevance include the liquid-phase oxidation of *para*-xylene to terephthalic acid, the acid hydrolysis of sodium salicylate to salicylic acid, and the absorption of ammonia in aqueous sulfuric acid to form ammonium sulfate, among others. There is a large amount of information in the literature on the experimental as well as theoretical aspects of reactive crystallization (Nielsen, 1964; Nyvlt et al., 1985; Söhnel and Garside, 1992; Mullin, 1993; Myerson, 1993; Tavare, 1995).

Precipitation is a complex phenomenon comprising simultaneous reaction, mass transfer, rapid nucleation and growth, as well as possible secondary processes of aging, ripening, agglomeration and breakage. Considerable advances have been made in understanding the interplay among these mechanisms. Garside and Tavare (1984) and Matsuoka and Garside (1993) discussed the transport of solute from the bulk solution to the crystal/solution interface and its subsequent incorporation into the crystal lattice. Franck et al. (1988) modeled salicylic acid precipitation, accounting for diffusion or kinetic limited crystal growth, primary and secondary nucleation, and growth by agglomeration of smaller crystals. Tavare and Garside (1990) investigated the effect of feed addition rate and Ostwald ripening on the crystal characteristics in a semi-batch reactive crystallizer with no mass-transfer limitations. Wachi and Jones (1991) analyzed a gas-liquid heterogeneous precipitation system by combining the film theory of gas-liquid mass transfer with the population balance equations for the precipitating solute. Their results clearly show the significant effect of mass transfer on the resulting crystal-size distribution. Mersmann and Kind (1988) and Franke and Mersmann (1994) examined precipitation from the viewpoint of process operations. The influence of operating conditions such as the mode of operation, feed location, residence time, reactant concentrations and power input on the overall process was studied. While providing significant insights and guidance for process design, all these previous investigations focused primarily on sparingly soluble systems and the reactive crystallizer was treated as an isolated unit operation.

Correspondence concerning this article should be addressed to K. M. Ng.

In contrast, Berry and Ng (1997) considered the design of a complete reactive crystallization flowsheet, based on an analysis of a reactive solid-liquid equilibrium (SLE) phase diagram. A design procedure was proposed for systems with multiple reactions and multiple phases. By choosing the proper reaction conditions and flowsheet configurations, the desired products can be manufactured with temperature and pressure swings, while suppressing the formation of undesirable byproducts. Relevant process paths are shown on the phase diagram as an aid for process conceptualization. This procedure is applicable to systems with all degrees of solubility. However, it is unclear how reaction kinetics, mass-transfer limitations, as well as nucleation and growth of crystals impact the equilibrium-based design.

The objective of this article is to extend the synthesis procedure by incorporating the various mechanisms into the conceptual design. It is shown that while thermodynamics dictates the ultimate limits of a reactive crystallization system, the kinetics of reaction, nucleation and growth, and the mass transfer determine the actual process paths leading to those limits. The phase behavior of crystallizing systems is discussed for reactive as well as nonreactive situations. A generic model which incorporates all simultaneous rate processes is then developed. The effects of the above individual mechanisms of kinetics and mass transfer on the process paths and the resulting crystal-size distribution are elucidated. The use of this approach for designing crystallizing systems is illustrated with suitable examples involving single as well as coprecipitation systems, and salting out precipitation.

The generic model developed in this article is applicable to reactions with any number of components. For ease of illustration, however, only examples with ternary or quaternary mixtures are used. This article deals with a continuous mixed suspension mixed product removal (MSMPR) crystallizer; nonideal mixing effects are not considered. We begin with a description of isothermal solid-liquid equilibrium (SLE) phase diagrams for quaternary mixtures.

Description of Solid-Liquid Phase Diagrams

Figure 1 shows the types of isothermal behaviors one might encounter for a quaternary mixture which can be represented on a tetrahedral phase diagram in mole-fraction coordinates. The solubility surfaces are shown as planes. Figure 1a shows the solubility surface for a solute P which is soluble in S but insoluble in A and Q. Any point on the solubility surface describes the concentration of P in equilibrium with the prevailing concentrations of A, Q, and S. If, in addition to S, A and Q also act as solvents for P, the solubility surface no longer passes through the vertices A and Q. Instead, it intersects the PA and PQ edges (Figure 1b). Here, points ps, pa, and pq represent the *single saturation points* of P with respect to S, A and Q, respectively. A composition within the region P-ps-pa-pq is saturated with respect to P, and will lead to precipitation of P. Figure 1c shows the case where either P or Q can potentially precipitate out. If the solubilities of P and Q are such that the two solubility surfaces intersect, then coprecipitation can occur (Figure 1d). Points 1 and 3 represent the solubilities of Q and P in A, respectively. Points 5 and 6 represent the solubilities of Q and P in S, respectively. The solubility surfaces of P and Q intersect to form the *double saturation trough*, line 24, where the composition is just saturated with respect to both P and Q. Any composition within the region $1245Q$ is only saturated with respect to Q. A composition lying in the region $3246P$ is saturated only with respect to P. Any composition below these two regions (prism $Q2P4$) is doubly saturated with respect to P and Q. Figure 1e shows the case where A, P, and Q have

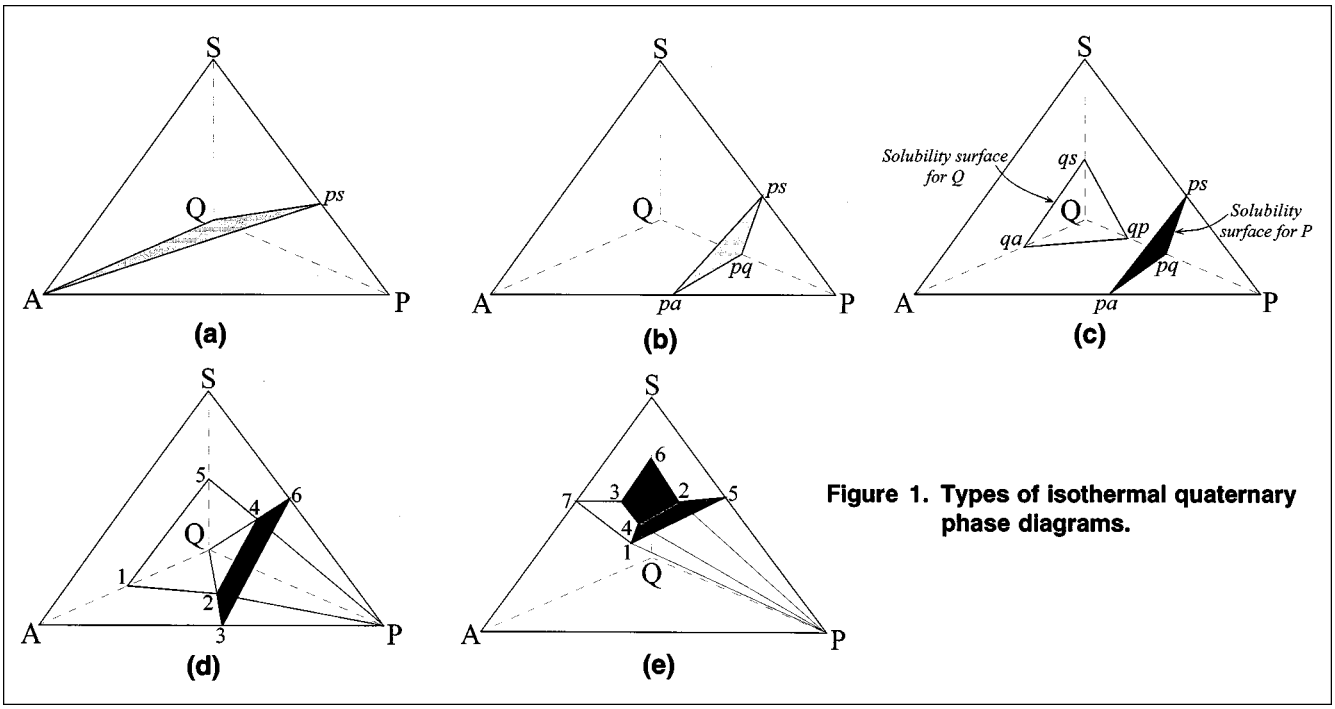

Figure 1. Types of isothermal quaternary phase diagrams.

limited solubility in *S*. Any composition above the three *single saturation surfaces* is unsaturated. There are three double saturation troughs: lines 14, 24, and 34. Point 4 is the *triple saturation point* where *A*, *P*, and *Q* coprecipitate. For each of the three solutes, there exists a region of saturation where the system is only saturated with a particular solute. For example, a composition lying in region 1425*P* is saturated only with respect to *P*. A composition lying within the region 4*APQ* is saturated with respect to *A*, *P*, and *Q*.

Equation for solubility surfaces

For design calculations, it is necessary to describe the solubility surfaces in the form of solubility equations. At a fixed temperature, the solubility C_P^* of a solute with units of moles of solute/m^3 of solution is in general a function of the concentrations of other species in the reaction mixture. If the solubility surfaces in a multicomponent system can be approximated by linear planes, at a given temperature, a general solubility equation for species *P* in the presence of *n* other species can be written as

$$C_P^* = \sum_{j=1}^{n} \left(\frac{1-\alpha_j}{\alpha_j} \right) C_j \qquad (1)$$

where α_j is the mole fraction of *j* in a saturated binary mixture of *j* and *P*. Thus, $(1-\alpha_j)/\alpha_j$ is the molar ratio representing the solubility of *P* in species *j* at the same temperature. If a certain component *i* does not act as a solvent for *P*, then $\alpha_i = 1$. Thus, $\alpha_A = \alpha_Q = 1$ for Figure 1a where *P* is insoluble in components *A* and *Q*. Equation 1 represents a hyperplane in $n+1$ dimensions. For this article, we shall be limited to the joint solubility of at most 4 species, which can be represented by a plane in a tetrahedral phase diagram.

SLE phase diagrams with equilibrium reactions

In the presence of a reaction, the complete phase diagram also includes a reaction equilibrium envelope. At constant temperature and pressure, the solid-liquid phase diagram with reaction can be calculated following the procedure outlined in Berry and Ng (1997). Figure 2a shows the complete phase diagram for the reacting system $A + B \leftrightarrow 2P\downarrow$ in the pres-

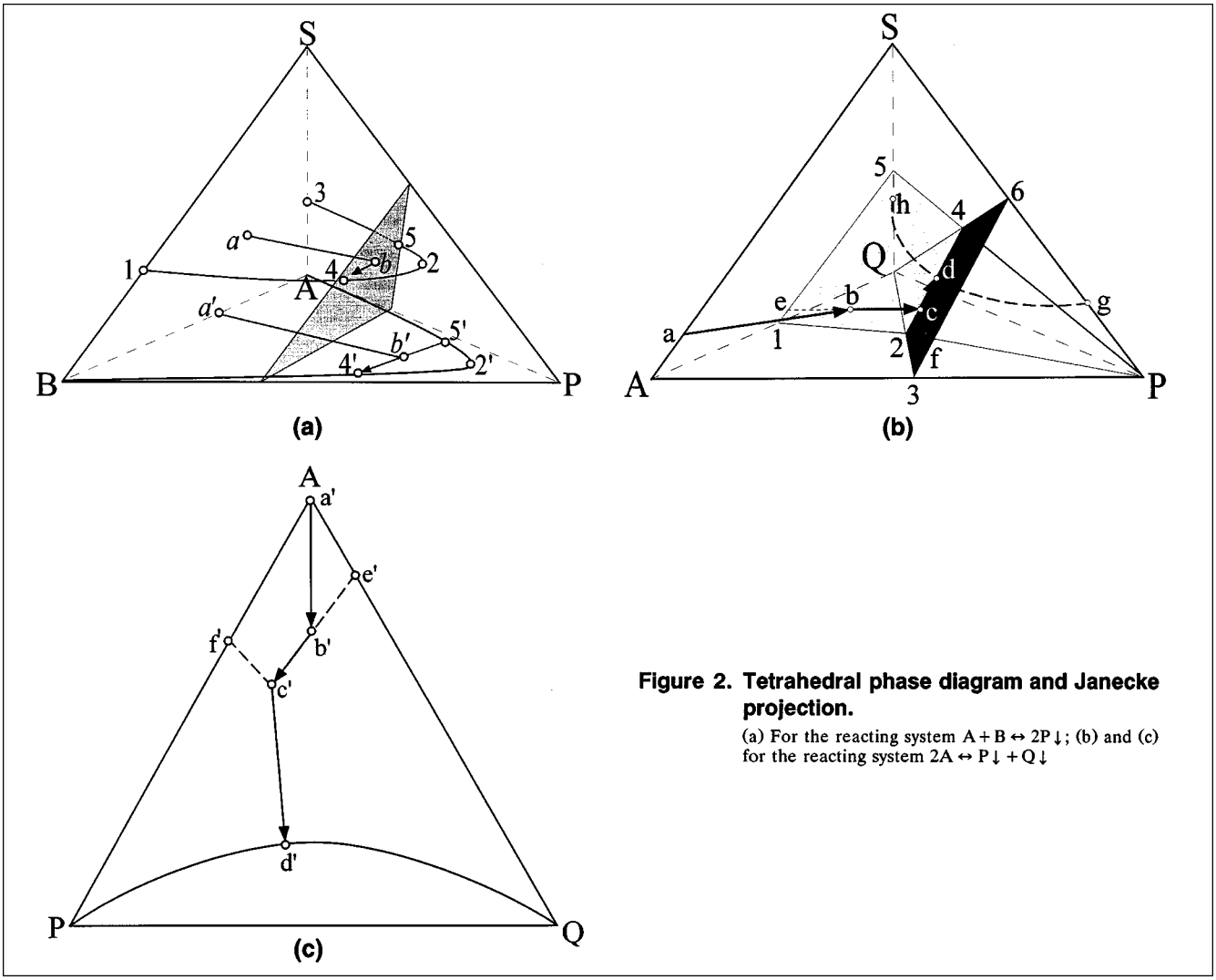

Figure 2. Tetrahedral phase diagram and Janecke projection.

(a) For the reacting system $A + B \leftrightarrow 2P\downarrow$; (b) and (c) for the reacting system $2A \leftrightarrow P\downarrow + Q\downarrow$

ence of an inert solvent S. The shaded triangle represents the solubility surface of P, described by the following solubility equation

$$C_P^* = \frac{3}{7}C_A + \frac{2}{3}C_B + \frac{2}{3}C_S \tag{2}$$

Note that the solubility surface was plotted in mole fraction coordinates, although the solubility equation is in terms of mol/m^3 of solution. The curve 123 represents a horizontal cut of the reaction equilibrium envelope at a certain solvent mole fraction. (The entire reaction equilibrium envelope can be generated by making a series of such sectional curves.) The equilibrium curve intersects the solubility surface at points 4 and 5. Starting with a composition at point a, the system moves along a line of constant stoichiometry ab as the reaction proceeds. At b, the system is saturated in P, and P crystallizes out. Under conditions of phase equilibrium, the solution composition then moves along path $b4$, until it reaches point 4 which satisfies both phase and reaction equilibrium.

The three-dimensional (3-D) phase relationships are more conveniently displayed on a 2-D Janecke projection, the construction of which has been reviewed elsewhere (Dye and Ng, 1995). Basically, the Janecke projection is a projection of any point in the tetrahedron onto the base of the tetrahedron, as viewed through the apex S. The Janecke projection for the above phase diagram is shown on the base of the tetrahedron. Thus, $B2'A$ and $5'b'4'$ represent the projections of the relevant portions of the equilibrium envelope and the solubility surface, respectively. A system composition within the region $B2'A$ will lead to a generation of P, while a composition beyond $B2'A$ will consume P to form A and B. A composition above the solubility line $5'4'$ (towards P) will crystallize P. For the above reaction system, $a'b'4'$ represents the Janecke projection of the process path, as the reaction proceeds with an initial concentration represented by point a'.

The Janecke projection for a two solute system is similar to the one described above. Consider a two solute system undergoing a reaction $2A \leftrightarrow P\downarrow + Q\downarrow$ in the presence of an inert solvent S. The complete phase diagram for this system including the reaction equilibrium envelope is shown in Figure 2b. The shaded regions represent the solubility surfaces of the two solutes, as described in Figure 1d earlier. The double saturation trough is shown by line 24. Curve gdh represents a horizontal cut of the reaction equilibrium envelope at a certain solvent mole fraction. The double saturation trough and the equilibrium envelope intersect at point d, which is the invariant point. Starting with a composition at point a, the system moves along a line of constant stoichiometry ab as the reaction proceeds. At b, the system is saturated in Q, which precipitates out. Under conditions of phase equilibrium, the composition then moves along line bc, which lies on the solubility surface of Q, until it hits the double saturation trough (point c). At point c, the system is saturated in P as well, which precipitates out. The system composition then moves along line cd until it reaches the reaction equilibrium envelope. The Janecke projection of the above phase diagram is shown in Figure 2c. Lines $f'c'$, $e'c'$ and $c'd'$ represent the projections of the relevant portions of the single saturation surfaces of P and Q, and the double saturation trough, respectively. The projection of the curve gdh is given by curve $Pd'Q$. For the above reaction, $a'b'c'd'$ represents the projection of the process path as the reaction proceeds.

On the Janecke projection, any composition within the region $Af'c'e'$ is unsaturated. Examination of the tetrahedral phase diagram in Figure 2b reveals that the Janecke projection of a portion of the single saturation region for Q (that is, region $1245Q$), and similarly for P (that is, region $3246P$), overlaps the projection of a portion of the double saturation region of P and Q (that is, region $Q2P4$). Thus, on the Janecke projection, a composition within the regions $Qe'c'd'Q$ ($Pf'c'd'P$) can either be saturated with only Q (P), or both Q and P, depending on the solvent content.

Generic Model for a Reactive Crystallizer

A generic model is now developed, which incorporates the effect of kinetics and mass transfer into the equilibrium-based design of reactive crystallization systems. The following mechanisms play a role in a reactive crystallization process. Reaction in solution results in supersaturation of the dissolved product, which leads to a formation of crystal nuclei. Mass transfer of the dissolved solute to existing crystals and incorporation of the solute into the crystal lattice leads to crystal growth. These mechanisms or steps proceed sequentially, and the overall rate is determined by the slowest step. This scenario can be further complicated by a gas-liquid reaction where gas-liquid mass transfer represents an additional step. In salting-out crystallization, the dissolution rate of a solid salting-out agent can be the rate-limiting step. Each of the above steps is characterized by a characteristic time, the ratios of which determine the relative rates of the different mechanisms. This is illustrated below using a salting-out reactive crystallization system.

Reactive crystallization with a solid reactant

Consider an MSMPR crystallizer being fed with a liquid feed stream containing reactant species A at a volumetric flow rate F. A solid reactant B is also charged continuously at a molar flow rate W. The solid reactant B dissolves and reacts with A in the liquid phase in the presence of an inert solvent S. The reaction is reversible in general even if the forward reaction is much faster than the reverse reaction. An amount of product P in excess of the solubility limit precipitates out of the solution as a solid product

$$\begin{aligned} B_{(s)} &\longrightarrow B_{(l)} \\ A_{(l)} + B_{(l)} &\longleftrightarrow 2P\downarrow \end{aligned} \tag{3}$$

The reaction rate can be generally given as a function of the concentrations of the reactant species

$$\mathcal{R}ate = \Phi(c) \tag{4}$$

The material balances for the reactant and product species can be set up as follows

Balance for Species A

$$F\left(C_A^f - C_A\right) - V\Phi = 0 \tag{5}$$

Balance for Species B

Liquid phase $$Vk_S a_S(C_B^* - C_B) - V\Phi - FC_B = 0 \tag{6}$$

Solid phase $$W - W\left(\frac{r}{r_0}\right)^3 - Vk_S a_S(C_B^* - C_B) = 0 \tag{7}$$

Balance for Species P

Liquid phase

$$F\left(C_P^f - C_P\right) + V\Phi - Vk_S a_T\left(C_P - C_P^s\right) - V\left(k_v \rho_m L_0^3\right) J_n = 0 \tag{8}$$

Liquid-crystal interface

$$Vk_S a_T\left(C_P - C_P^s\right) - V\left(a_T/2\right)\rho_m G = 0 \tag{9}$$

Here, C_P is the concentration of the dissolved solute in the bulk of the liquid, C_P^s is the concentration of the solute at the liquid-crystal interface, and C_P^* is the solubility. Note that the nucleation rate (J_n) (number/m^3· A) and the linear growth rate (G) (m/s) have been transformed into molar units by using appropriate multiplying factors. Examination of Eqs. 5 to 9 reveals five distinct rate steps: dissolution of B, reaction between A and B, the generation of P nuclei in the liquid phase, the mass transfer of dissolved P to the growing P crystals, and the surface integration of the solute P into the crystal lattice (that is, the crystal growth step). The relative importance of each of these steps can be characterized by a dimensionless number. For a reaction which is second order overall, and for nucleation and growth kinetics which can be represented by conventional power law expressions, we have

$$\Phi = k_2\left(C_A C_B - \frac{C_P^2}{K}\right) \tag{10}$$

$$J_n = k_n\left(C_P - C_P^*\right)^n \tag{11}$$

$$G = k_g\left(C_P^s - C_P^*\right)^g \tag{12}$$

The dimensionless numbers for the individual steps are then as follows

Reaction

$$Da_R = \frac{\text{Reaction Rate}}{\text{Reactor Throughput}} = k_2 C_A^f \tau \tag{13}$$

Dissolution

$$Da_D = \frac{\text{Reaction Rate}}{\text{Dissolution Rate}} = \frac{k_2 C_A^f}{k_S a_S} \tag{14}$$

Mass transfer

$$Da_M = \frac{\text{Reaction Rate}}{\text{Mass-Transfer Rate from Bulk to Crystal Face}} = \frac{k_2 C_A^F}{k_S a_T} \tag{15}$$

Nucleation

$$N_{Nu} = \frac{\text{Nuclei Generation Rate}}{\text{Reaction Rate}} = \frac{\left(k_v \rho_m L_0^3\right) k_n C_P^{*\,n-1}}{k_2 C_A^f} \tag{16}$$

Crystal Growth

$$N_{Gr} = \frac{\text{Surface Integration Rate}}{\text{Mass-Transfer Rate from Bulk to Crystal Face}} = \frac{\left(a_T/2\right)\rho_m k_g C_P^{*\,g-1}}{k_S a_T} \tag{17}$$

Note that the exact form of the dimensionless numbers would change according to the reaction kinetics, the growth rate expressions, and the mechanism chosen for nucleation, such as primary or secondary nucleation.

The dimensionless numbers as defined above represent the ratios of the rates of two consecutive steps. Similarly, by examining an appropriate product of dimensionless numbers, it is possible to identify the slower of any two nonconsecutive steps. For example, the ratio Da_R/Da_D compares the dissolution rate to the reactor throughput; the product $Da_R N_{Nu}$ compares the nucleation rate with the reactor throughput.

Range of parameter values in reactive crystallization systems

It is desirable to identify typical values for the dimensionless numbers involved in the generic reactive crystallizer

Table 1. Range of Parameters in Reactive Crystallization with First-Order Kinetics

k_1	10^{-6}–1.0	
τ	10^{2}–10^{4} s	
k_s	10^{-4}–10^{-2} m/s	
C^*	$10^{-4}\times10^{3}$ mol/m^3	(for high solubility compounds)
	0.01–10 mol/m^3	(for low solubility compounds)
k_g	10^{-13}–10^{-8} (m/s)/(mol/m^3)^g	
g	0.5–2	
k_n	0.1–1.0 no./[m^{3}s(mol/m^3)^n]	
n	1–5	
n_0	10^{13}–10^{18} no./m^4	
L_0	10^{-9}–10^{-7} m	
G	10^{-7}–10^{-8} m/s	(for high solubility compounds)
	10^{-9}–10^{-11} m/s	(for low solubility compounds)
Da_R	10^{-4}–1	
Da_M	10^{-6}–1	
Da_D	10^{-6}–1	
N_{Nu}	10^{-1}–10^{-7}	(for high solubility compounds)
	10^{-7}–10^{-15}	(for low solubility compounds)
N_{Gr}	1–10	(for high solubility compounds)
	10^{-3}–0.1	(for low solubility compounds)

model developed above. Table 1 provides such estimates for a system with first-order reaction kinetics. Also presented are reaction, mass-transfer, nucleation, and growth parameter values, the solubility, and the residence time from which the dimensionless numbers were derived. Most of the data, primarily based on inorganics, were obtained from a survey by Mersmann and Kind (1988) on reactive as well as nonreactive industrial crystallization systems. Additional data were culled from Sohnel and Garside (1992). The estimated dimensionless numbers cover a wide range, partly because they incorporate the range of the reaction kinetic constant k_1. For high solubility compounds such as KNO_3, NaCl, and $(NH_4)_2SO_4$, the growth number is on the order of 1 to 10, whereas it ranges from 10^{-3} to 0.1 for sparingly soluble compounds such as BaC_2O_4, $CaCO_3$ and $BaCO_3$.

One of the steps often controls the overall rate of the reactive crystallization process, although the driving forces adjust themselves so that the rate of each individual step is equal to the overall rate at steady state. This controlling step can be identified by carrying out a sensitivity analysis of the generic model. (For example, see Kelkar and Ng (1998) for a similar sensitivity analysis for gas-liquid and gas-liquid-solid catalytic reactions.) An identification of the controlling step provides insights for increasing the productivity of the crystallizer and for tuning the properties of the crystallizing solute, such as its crystal-size distribution. It is interesting to examine the crystallizer performance, when a mechanism is much faster or slower compared to the step adjacent to it.

Example 1: crystallizer performance for a condensed ternary system with a solid reactant and a single crystallizing solute

Consider the reaction between A (which also acts as solvent) and dissolved solid B to yield P which crystallizes out (Eq. 3). We examine situations where a dimensionless number is close to its upper or lower limits, so that it has a dominating effect on the crystallizer performance. Figure 3 shows the results for such a simulation for a crystallizer with a volume of 0.1 m^3. The properties of interest are the dominant crystal size L_d (μm), which corresponds to the maximum of the weight fraction distribution, the supersaturation $C_P - C_P^*$, the concentration difference $C_P - C_P^s$ between the bulk of the solution and the crystal face, and the production rate M_c (kg/h) of crystals. The base case is for high rates of reaction, dissolution, mass transfer and crystal growth, and a low rate of nucleation. The values of the reaction, mass transfer and dissolution Damköhler numbers, and the nucleation and growth numbers used for the different cases are given in Table 2. Note that the values of the mass-transfer Damköhler number Da_M, and the dissolution number Da_D, are calculated from the model, because the surface area of the crystals a_T and that of the dissolving solid reactant a_S are *a priori* unknown. These Damköhler numbers are controlled by choosing an appropriate value of the solid-liquid mass-transfer coefficient k_S.

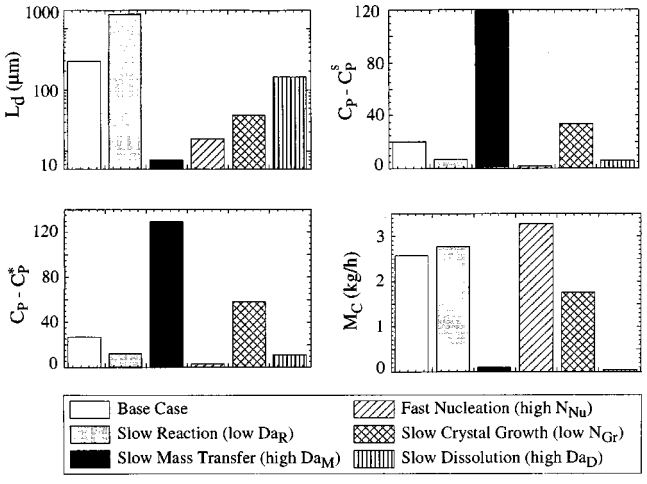

Figure 3. Crystallizer performance for different dominating mechanisms.

Table 2. Parameter Values for Simulations with Different Dominant Mechanisms

Dominating Mechanism	Da_R	Da_M	Da_D	N_{Nu}	N_{Gr}
Base case	200	31	89	1×10^{-14}	1
Slow reaction	40	2	16.7	1×10^{-14}	1
Slow mass transfer (of solute from bulk to crystal)	200	880	62	1×10^{-14}	1
Fast nucleation	200	.01	100	1×10^{-4}	1
Slow crystal growth	200	78	79	1×10^{-14}	.01
Slow reactant dissolution	200	3600	1001	1×10^{-14}	1

The chart for L_d shows that the largest crystals are obtained for an operation involving a slow reaction (low Da_R). This is because, for a low reaction rate, the mass transfer does not limit the overall process, and, hence, excessive levels of supersaturation do not exist (as evidenced by the low value of $C_P - C_P^*$ for slow reaction operation). This leads to the formation of a limited number of nuclei which can then grow to a large size.

On the other hand, when the mass transfer of the solute from the bulk to the liquid-crystal interface is much slower than the reaction (high Da_M), it results in a large value of $C_P - C_P^s$, as well as the supersaturation $C_P - C_P^*$. This leads to excessive nucleation, and, hence, a smaller dominant crystal size. Also, since the slow mass transfer limits the amount of solute incorporated into the crystals, the output of crystals M_C is low.

For an operation with a high nucleation rate ($N_{Nu} = 10^{-4}$), whatever supersaturation is generated is quickly relieved by the formation of new nuclei, as seen by the very low values of $C_P - C_P^s$ and $C_P - C_P^*$. A low supersaturation leads to low growth rates, and, hence, small-sized crystals. The crystal output M_C is, however, large. Similarly, when the rate of crystal growth is very low ($N_{Gr} = 0.01$), the dominant crystal size is smaller than that in the base case.

Lastly, consider a process where the dissolution of one of the reactants, which could also be the salting-out agent, is a slow operation (high Da_D). Since only a limited amount of reactant is available to react, the overall rate of reaction is small and the crystal output (0.01 kg/h) is low. However, large crystals can be obtained owing to the limited supersaturation.

Table 3. Parameter Values Used for Simulations (Unless Otherwise Specified)

Examples 2 to 6			
N_{Nu}	10^{-8}	k_v	0.52
N_{Gr}	0.1	L_0	10^{-7} m
n	4	ρ_m	20,000 mol/m^3
g	2		

Examples 2 and 4		Example 5		Examples 3 and 6	
k_2	10^{-3} m^3/mol·s	k_2	10^{-3} m^3/mol·s	k_1	0.01 s^{-1}
K	10	K	10	K	100
k_S	0.001 m/s			k_S	0.0005 m/s

Kinetic and Mass-Transfer Effects on Process Paths

It is necessary to couple the individual steps occurring during reactive crystallization with the reaction and solid-liquid phase equilibrium, which ultimately decide the limits of the precipitation process. The effect of the dimensionless numbers on the process paths is illustrated below with examples. The parameter values used in the following simulations are given in Table 3, unless otherwise specified.

Example 2: condensed ternary system with a single crystallizing solute

Consider a ternary system of components A, B and P that undergoes the following reaction in solution

$$A + B \longleftrightarrow 2P \downarrow \tag{18}$$

where P is sparingly soluble in A and B, which act as the solvent. Several characteristics of such a system will now be discussed.

Process path for increasing Da_R

For an isothermal, isobaric, condensed (that is, negligible vapor pressure) system with a single reaction, the degree of freedom is zero (Berry and Ng, 1997). Figure 4 shows the ternary phase diagram in mole fraction coordinates for this system with $K = 10$. The reaction equilibrium curve is $A1B$. Line 26 gives the solubility of P for all solution compositions, and is given by Eq. 1 with $\alpha_1 = \alpha_2 = 0.5$, that is

$$C_P^* = C_A + C_B \tag{19}$$

If the dependence of solubility on A and B were different, the solubility line would change accordingly. The invariant points 3 and 5 are the intersection points of the reaction equilibrium and solubility curves, and, thus, are the two stable nodes of the system. Triangle $P26$ represents compositions which are saturated in P, whereas the region below the solubility line represents unsaturated solutions. For a given inlet composition, it is interesting to track the path of the system for an increasing reaction Damköhler number Da_R in an MSMPR reactive crystallizer. Curve *abcd* shows one such path for an inlet composition of 55% A and 45% B. The portion *ab* of the path represents those Da_R values for which the crystallizer is still unsaturated in P. The system becomes saturated in P at a sufficiently high Da_R, but crystallization

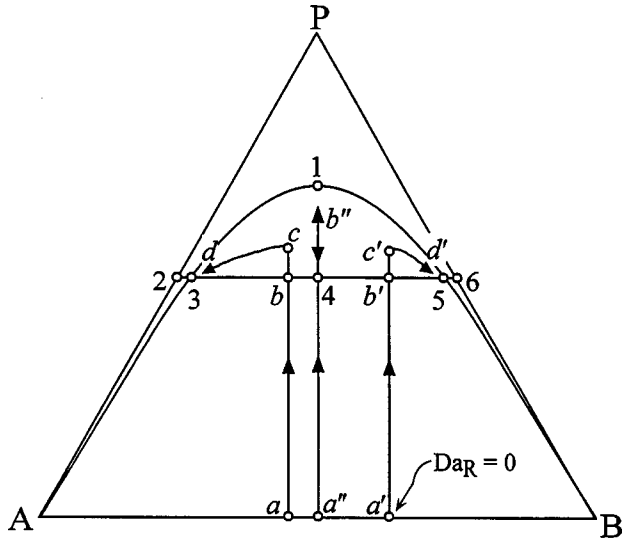

Figure 4. Process paths for an increasing reaction Damköhler number.

does not commence until point c. A supersaturation represented by b-c is required to achieve the nucleation and growth rates required for significant crystallization to occur. If the reaction Damköhler number is further increased, the process path turns and proceeds to invariant point 3. For an initial composition consisting of 37% A and 63% B, the system moves along path $a'b'c'd'$ until it reaches the invariant point 5. Point 4 is the saddle point. A system with equal amounts of A and B in the inlet will move along line $d''4b''$, before moving back to point 4 where a complete conversion to solid P occurs. The process paths for an increasing Da_R can also be interpreted as the progress of the composition of a batch reactive crystallizer in time.

Effect of growth number

Consider the same ternary system with a certain concentration of P, C_P in the bulk of the solution. There is a mass transfer of P from the bulk to the vicinity of the growing crystals, where the concentration of P is C_P^s. Here, P is eventually incorporated into the crystal lattice. The growth number N_{Gr}, defined by Eq. 17, gives the relative rate of crystal growth with respect to the rate of mass transfer of the solute to the liquid-crystal interface. For given mass-transfer conditions, a higher growth number indicates a higher growth rate for the crystals, and correspondingly, a C_P^s closer to C_P^*, that is, a system closer to phase equilibrium. Figure 5 shows the process paths of the system with increasing Da_R for different growth numbers. The system lies closer to the solubility line 23 with increasing N_{Gr}. In other words, a lower N_{Gr} requires a higher driving force for crystal growth, thus moving the system away from the solubility line. All paths eventually end at point 2, which is the intersection of the solubility line with the reaction equilibrium curve.

Effect of mass-transfer Damköhler number

We next consider the effect of the mass-transfer Damköhler number Da_M on the process path. The P produced by the reaction is transferred to the liquid-crystal interface, and the

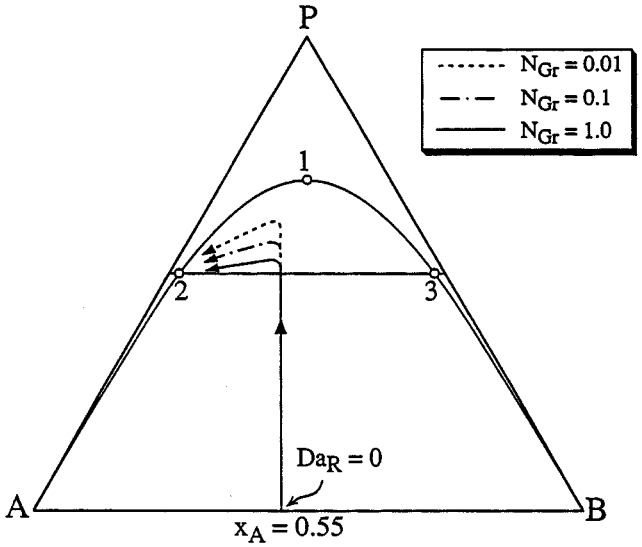

Figure 5. Process paths for different growth numbers.

mass-transfer Damköhler number, defined by Eq. 15, gives the ratio of the rates of these two consecutive steps. The lower the Da_M, the faster is the mass-transfer relative to the reaction, and *vice versa*. Thus, for a lower Da_M, the concentration in the vicinity of the crystals C_P^s is closer to the concentration in the bulk C_P. For a given crystal growth number, a lower Da_M implies a system closer to the solid–liquid phase equilibrium. Figure 6 shows the process paths of a system with an inlet composition of 45% *A* and 55% *B* for different Da_M. As Da_M increases, the path ventures further and further away from the solubility line before turning back to meet point 3. Mass transfer then becomes the limiting step in the overall process, leading to a buildup of supersaturation and excessive nucleation. Note that Da_M is not constant along a given path of increasing Da_R. This is because the crystal surface area a_T changes as the crystallization proceeds.

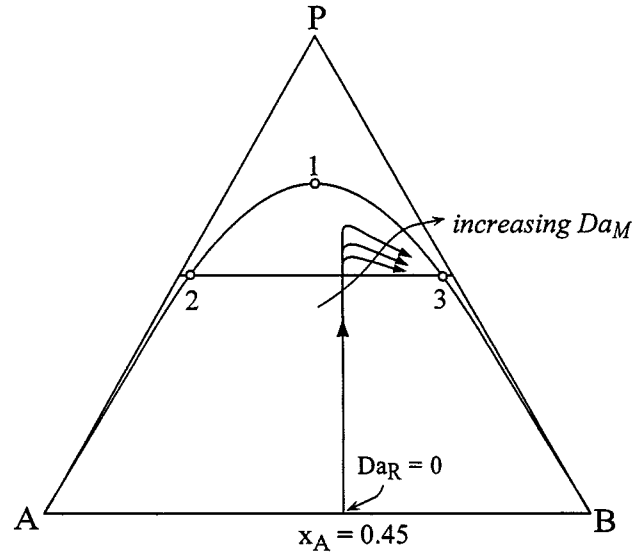

Figure 6. Process paths for different mass-transfer Damköhler numbers.

Effect of nucleation number

The nucleation term in the mass balance for the crystallizer accounts for an insignificant portion of the total mass, because of the small size of the nuclei. However, the nucleation rate does significantly affect the system concentrations and other properties through the supersaturation. For the same ternary system, we now consider the effect of the nucleation number N_{Nu} on the characteristics of the crystals produced by the system. The nucleation number N_{Nu}, defined by Eq. 16, gives the rate of nucleation relative to the rate at which *P* is produced by the reaction. A higher N_{Nu} implies a larger number of nuclei and thus a higher number density of smaller crystals. For an MSMPR crystallizer, the weight fraction distribution is an analytical expression given as (Randolf and Larson, 1988)

$$w(L) = \frac{L^3 \exp(-L/G\tau)}{6(G\tau)^4} \tag{20}$$

Figure 7a shows the weight fraction distribution of the crystals in the solution for three different values of N_{Nu}. For this simulation, $k_2 = 10^{-2}$ m^3/mol·s, and $K = 6$, the other parameters being given by Table 3. For $N_{Nu} = 10^{-6}$, the dominant particle size corresponding to the maximum of the distribution occurs at 24 μm. The distribution is rather narrow, indicating that none of the crystals have sufficient time to

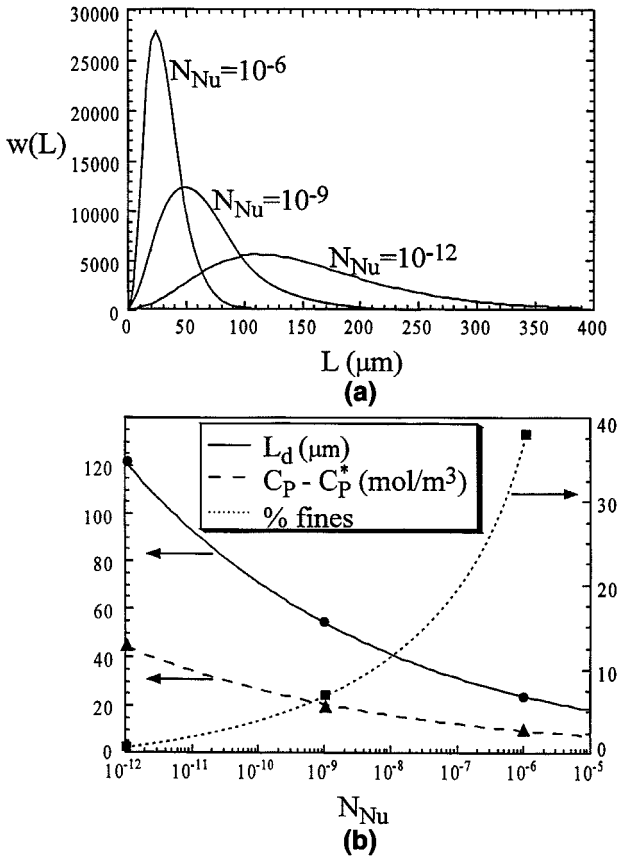

Figure 7. Effect of the nucleation number on crystallizer performance.

grow. For a lower nucleation number ($N_{Nu} = 10^{-12}$), the distribution is wider with a dominant crystal size of 121 μm. Figure 7b shows that the dominant particle size, as well as the supersaturation in the system, decreases with an increase in N_{Nu}. Considering crystal sizes below 25 μm as fines, we can obtain the wt. % of fines in the system by integrating the weight fraction distributions from size 0 to 25 μm. Figure 7b shows that as N_{Nu} increases from 10^{-12} to 10^{-6}, the percentage of fines rises from about 0.4% to 38%. It is clear that the nucleation rate should be controlled tightly to obtain good sized crystals.

Example 3: condensed quaternary system with two crystallizing solutes and a solvent

Many reactions take place in the presence of an inert solvent. Also, it is possible for more than one solid to crystallize in a reactive crystallization process. Consider a quaternary system composed of reactant A which undergoes the following reaction in an inert solvent S under isobaric and isothermal conditions

$$2\,A \longleftrightarrow P\downarrow + Q\downarrow \tag{21}$$

Here, P and Q can precipitate out from the solution. Consider the following solubility surfaces for P and Q

$$C_P^* = \frac{1}{2}C_A + \frac{2}{3}C_S \tag{22a}$$

$$C_Q^* = \frac{1}{4}C_A + \frac{2}{3}C_S \tag{22b}$$

The tetrahedral phase diagram and the Janecke projection of the same was described earlier (Figures 2b and 2c). The MSMPR model for this system is set up as before. The system is nondimensionalized by defining a reaction Damköhler number Da_R, two mass-transfer Damköhler numbers ($Da_{M,P}$ and $Da_{M,Q}$), two nucleation numbers ($N_{Nu,P}$ and $N_{Nu,Q}$), and two crystal growth numbers ($N_{Gr,P}$ and $N_{Gr,Q}$) for P and Q. The meaning of all the dimensionless numbers remains the same as before. The effect of the dimensionless numbers on the process path for an increasing Da_R will be discussed below.

Effect of growth numbers

Consider the progress of a system with only A and S at the inlet for increasing reaction Damköhler numbers. Figure 8 shows the Janecke projection of two such paths for different values of growth numbers for P and Q. Since Q has the lesser solubility of the two, it crystallizes first (points b and b'). Once the paths cross the double saturation trough, the system is saturated with P as well (points c and c'). For increasing Da_R, the system approaches point 4′ which is the intersection of the double saturation trough with the reaction equilibrium envelope. The growth rates for P and Q are higher for the system following path $abcd$ than for that following path $a'b'c'd'$. As explained in Example 2, the higher the growth rates, the closer the system is to phase equilibrium. Thus, curve abc lies closer to the solubility line of Q than curve $a'b'c'$, and curve cd lies closer to the double saturation trough than curve $c'd'$.

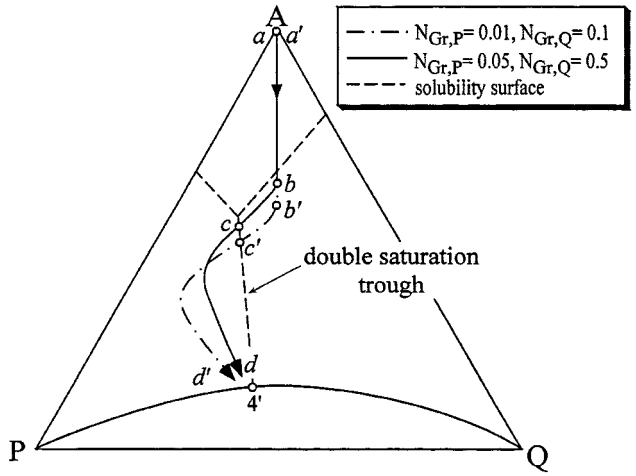

Figure 8. Effect of the crystal growth number on the process paths for a two solute system.

Effect of mass-transfer Damköhler numbers

Consider the same reaction as above yielding the two solutes P and Q, but the system now has a symmetrical solubility profile given by the equations

$$C_P^* = \frac{1}{4}C_A + \frac{2}{3}C_S \tag{23a}$$

$$C_Q^* = \frac{1}{4}C_A + \frac{2}{3}C_S \tag{23b}$$

Figure 9 shows the process paths (for an increasing Da_R) taken by the system for different mass-transfer Damköhler

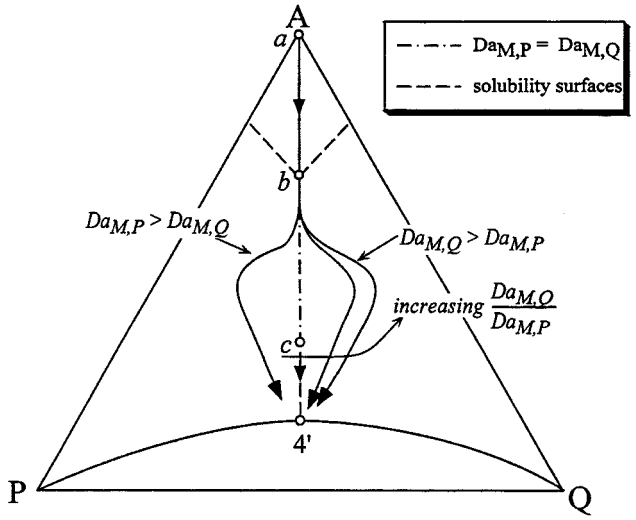

Figure 9. Effect of the mass-transfer Damköhler number on process paths for a two solute system.

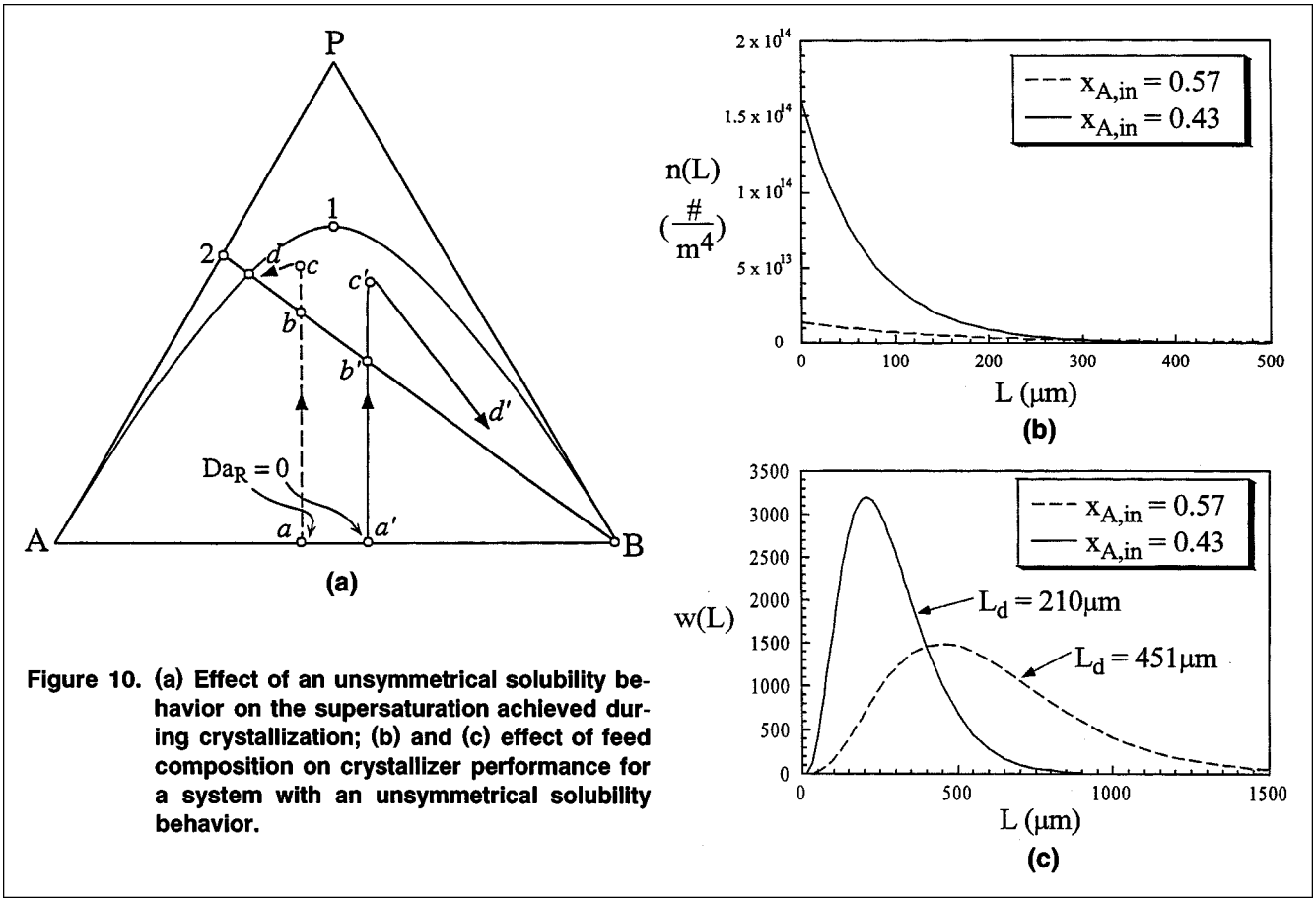

Figure 10. (a) Effect of an unsymmetrical solubility behavior on the supersaturation achieved during crystallization; (b) and (c) effect of feed composition on crystallizer performance for a system with an unsymmetrical solubility behavior.

numbers $Da_{M,P}$ and $Da_{M,Q}$. When $Da_{M,P} = Da_{M,Q}$, the system follows a path *abc*, just below the double saturation trough. For $Da_{M,P} > Da_{M,Q}$, the mass transfer of *Q* is faster than that of *P*. Thus, more of *Q* gets incorporated into the solid phase. But, since equal amounts of *P* and *Q* are being produced by reaction, there is a buildup of *P* in the solution and, hence, the process path lies in the left half of the Janecke projection. Similarly, for $Da_{M,Q} > Da_{M,P}$, the system compositions lie in the right half of the Janecke projection. Again, the larger the Damköhler number, the more severe the mass-transfer limitations are, and the farther the system ventures from phase equilibrium.

Crystallization Design Incorporating Kinetic and Mass-Transfer Effects

The utility of the present approach in the design of reactive crystallization systems is now discussed with examples involving single and coprecipitation systems, and a salting-out crystallization system. The parameter values used in the following simulations are given in Table 3, unless otherwise specified.

Example 4: controlling the CSD by manipulating inlet composition

It was demonstrated in Example 1 that excessive supersaturation leads to an undesirable crystal-size distribution. How far the system ventures into the supersaturated region depends on the solubility limit and the crystallization kinetics of the solute, but the system is also limited by the reaction equilibrium envelope, which it cannot cross. We can take advantage of this fact to control the supersaturation in a system, and thus tailor the crystal-size distribution to our needs. Figure 10a shows the phase diagram of the same ternary reacting system as described in Example 2, but with a nonsymmetrical solubility profile (line 2B) as given by the equation

$$C_P^* = \frac{2}{3} C_A \qquad (\text{where } \alpha_A = 0.6, \text{ and } \alpha_B = 1.0) \quad (24)$$

With an increasing amount of *A* relative to *B*, the solubility line comes closer and closer to the equilibrium curve (curve *A*1*B*). Thus, the maximum supersaturation which can be achieved in the system is lesser for a system with more *A* than *B*. The curve *abcd* shows the process path for increasing Da_R for a system with an inlet composition of 57% *A* and 43% *B*. The maximum supersaturation developed is represented by *b*-*c*. The curve *a*′*b*′*c*′*d*′ is the process path for a system with an inlet composition of 43% *A* and 57% *B*. Since the solubility line lies far below the reaction equilibrium curve, the maximum supersaturation developed here, *b*′-*c*′, is higher than in the earlier case. Figure 10b shows the crystal number density distribution for the two cases. The higher supersaturation in the latter system leads to a larger nucleation

rate. This is evident from the fact that n_o, the population density of nuclei, which also characterizes the nucleation rate, is much higher for the latter system. Figure 10c shows the weight fraction distributions for the crystals produced by the two systems. For the system with the lower supersaturation, the distribution is broader, with a dominant particle size of 451 μm. For the system with the higher supersaturation, the dominant particle size is only 210 μm. This demonstrates that the crystal-size distribution can be adjusted by making a wise choice of the inlet concentrations.

Example 5: eliminating mass-transfer limitations in salting-out reactive crystallization

In some reactive crystallization processes, one of the reactants could be a solid which serves as a salting-out agent. The rate of dissolution of the solids should be sufficiently fast so that no undissolved salting-out agent particles can leave the crystallizer. The rate of solid dissolution depends on several factors, namely: rate of reaction, the solid-liquid mass-transfer coefficient, salting-out agent solubility, and the average size of the particles being charged. Depending on the values of the above variables, the dissolution rate could be slow enough that the crystallization process is limited by the dissolution. A design criterion is presented to identify presence of dissolution limitations, and to choose the value of design variables such as the size of the solid particles being charged.

Consider a reaction taking place between A in solution and the dissolved salting-out agent B to form the sparingly soluble product P in an MSMPR crystallizer (Eq. 3). Assume that the particles being charged are all of the same size. Also, since the solids are in a perfectly mixed state, all particles in the crystallizer are of the same size. Figure 11 plots the percentage of undissolved solid as a function of the dissolution number (Eq. 14) for a case as shown in the inset. We would like to operate at a low Da_D so that no undissolved solid particles leave the crystallizer. However, due to the assumption of perfect mixing in the crystallizer model, this criterion will lead to an infinitely large crystallizer (Rajagopal et al., 1988). Hence, for preliminary design purposes, we propose a criterion that the size of solid particles in the crystallizer be maintained below a certain value, say $r/r_0 < 0.1$. It is assumed that provided r/r_0 is sufficiently low, the deviation from a perfectly mixed flow pattern in an actual crystallizer will allow complete dissolution of all solids.

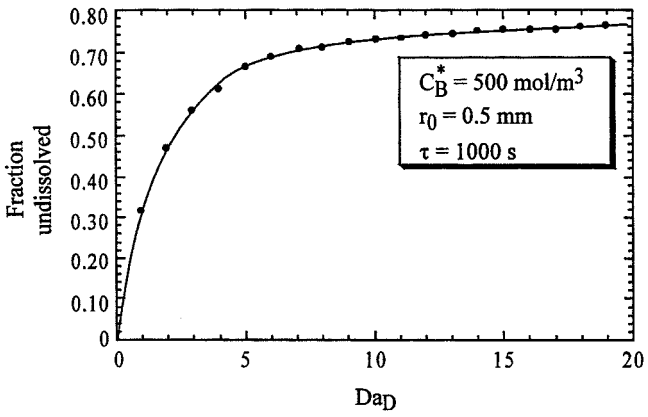

Figure 11. Percentage of undissolved solids as a function of the dissolution number.

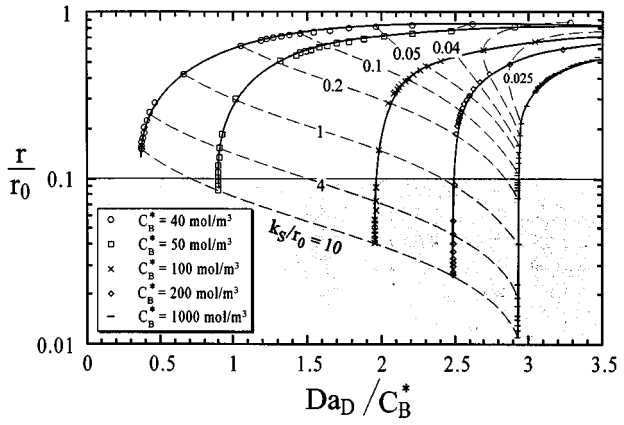

Figure 12. Chart for identifying presence of dissolution limitations during crystallization involving a solid reactant.

Recall that the higher the dissolution number, the slower is the rate of dissolution relative to the reaction rate. The dissolution rate is also proportional to the salting-out agent solubility, and, hence, the appropriate parameter to assess the presence of dissolution limitations is Da_D/C_B^*. For the above reacting system with stoichiometric amounts of solids charged, Figure 12 shows a plot of r/r_0 as a function of Da_D/C_B^*, with the solid solubility C_B^* as a parameter. The shaded region for $r/r_0 < 0.1$ indicates the region in which all solid particles are completely dissolved in a real crystallizer. The dashed lines are lines of constant k_s/r_0, and the solid ones are lines of constant C_B^*. Along a line of constant C_B^*, the dissolution limitations increase with increasing Da_D/C_B^*, or decreasing k_s/r_0. The lines of constant solubility and constant k_s/r_0 form a grid, which spans the entire range of r/r_0, from 0 to 1.

Two design situations for which the above plot can be used are identified. One is when we wish to identify whether dissolution limitations exist in an existing crystallizer, and the second is when we want to design a new crystallizer so that dissolution does not limit the overall process. For an existing crystallization system, knowing C_B^*, the solid–liquid mass-transfer coefficient k_s, and the radius r_0, one can immediately obtain the value of r/r_0. If $r/r_0 > 0.1$, then dissolution is probably limiting the overall process. Similarly, to design a crystallization system so as to not have dissolution limitations, one can proceed as follows. Knowing the solid solubility C_B^*, we can identify the range of k_s/r_0, for which $r/r_0 < 0.1$. This is the target region in which we want to operate. For example, for $C_B^* = 100$ mol/m^3, we should operate in the region $k_s/r_0 > 4$. Knowing the type of crystallizer, or by some minimal experimentation, k_s can be determined. Thus, a choice of the particle size r_0 can be made such that dissolution limitations do not exist.

Example 6: selective nucleation by seeding

Secondary nucleation involves the generation of new nuclei due to the presence of the solid phase of the crystallizing

solute itself. This is often achieved by seeding the crystallizer with microcrystals of the solute to be crystallized (Rousseau and O'Dell, 1980). The seed crystals can participate in the nucleation in several ways (Nyvlt et al., 1985). For example, tiny crystallites detached from the seed crystals may act as crystallization centers (apparent secondary nucleation), new nuclei may be formed as a result of crystal-solution interaction (true secondary nucleation), or crystal-crystal, crystal-impeller, and crystal-wall collisions may give rise to new nuclei (contact nucleation). If the rate of nucleation is modeled using an effective nucleation rate constant which incorporates all the mechanisms for primary as well as secondary nucleation, a nucleation number similar to the one defined earlier (Eq. 16) can be defined. A seeded crystallizer will lead to a higher nucleation number, and, hence, a higher nucleation rate, even at lower supersaturations. Altering the nucleation number by a method such as seeding may be especially useful in situations where coprecipitation occurs. The solute which has a higher nucleation number will crystallize in larger amounts, as discussed in the following example.

Consider the reaction $2A \leftrightarrow P\downarrow + Q\downarrow$ where A is the only solvent. Figure 13 shows the phase diagram of this ternary system. Lines $3Q$ and $1P$ represent the solubilities of P and Q in the system, respectively, and are given by the following equations

$$C_P^* = \frac{2}{7} C_A \tag{25a}$$

$$C_Q^* = \frac{3}{17} C_A \tag{25b}$$

Consider that P is the desired product. From the phase diagram, it is clear that the solubility behavior is contrary to the desired objective of selectively crystallizing P. This may be overcome by seeding the crystallizer with crystals of P, and thus increasing the nucleation number of P to be much larger than that of Q. Starting with pure A, path $abcd$ tracks the solution composition for an increasing Da_R. At point b, the system becomes saturated in Q. However, due to the low nucleation number of Q, it remains in solution. At point c, the system becomes saturated in P as well. The high nucleation number of P allows crystallization to occur at very low supersaturations. The solution composition moves along path cd, while Q, though in excess of its saturation value, remains in solution. Table 4 shows the results of the above process for a Da_R of 1,200 s, which corresponds to point d. The nucleation rate of P is four orders of magnitude higher than that of Q. The values of M_c, the crystal production rate, and a_T (m^2/m^3), the crystal surface area per unit suspension volume, indicate that while P has crystallized considerably, Q has just begun to nucleate. Increasing the Da_R will result in increasing crystallization of Q. Thus, selective crystallization of a solute is possible by suitably altering the nucleation numbers. Note that an analysis at phase equilibrium conditions would have predicted a crystallization of the undesirable product Q at point b with the solution composition moving along path $b2$.

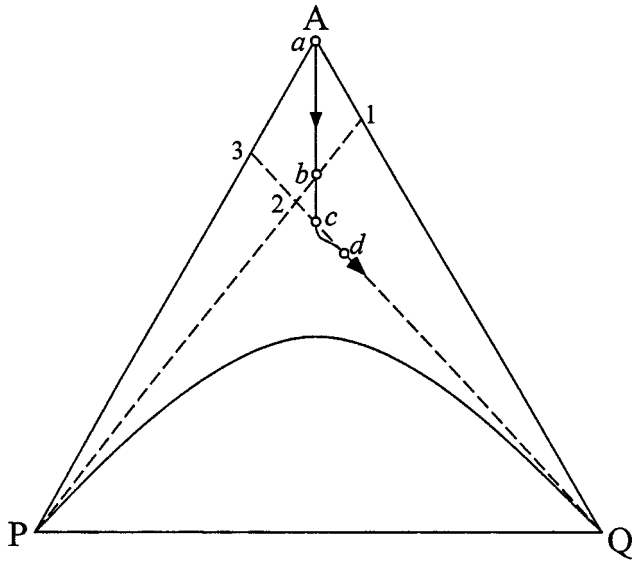

Figure 13. Process path for a two solute system with widely varying nucleation numbers.

Table 4. Crystallizer Performance for a Coprecipitating System Involving Selective Nucleation by Seeding

	P	Q
N_{Nu}	10^{-5}	10^{-12}
J_n (no./m^3s)	0.29×10^8	0.3×10^4
$C - C^*$ (mol/m^3)	1.43	36.17
a_T (m^2/m^3)	0.11×10^5	0.43
M_C (kg/h)	0.2	0

Conclusions

Recently, a number of equilibrium-based methods have been developed for crystallization system synthesis (Cisternas and Rudd, 1993; Dye and Ng, 1995; Berry and Ng, 1997; Cisternas and Swaney, 1998). Based on the solid-liquid phase behavior which is often presented with phase diagrams, process configurations involving crystallizers, dissolvers, filters, and so on are generated for separating a multicomponent mixture. In this article, reaction kinetics, crystallization kinetics, and mass-transfer effects are incorporated into the equilibrium-based approach.

This is critical because kinetics and mass-transfer effects determine the actual process paths as crystallization occurs. Based on the equilibrium analysis, a process path is given only by the interaction between the solubility and reaction equilibrium surfaces. In reality, the process path ventures deep beneath the solubility surface to create the necessary supersaturation for crystal nucleation and growth. Coupling the reaction and mass-transfer effects with the solubility and reaction equilibrium surfaces provides insights for process improvements. For example, by suitably altering the nucleation number in a coprecipitating system, we can selectively crystallize the desired solute, even though the equilibrium analysis indicates otherwise due to an unfavorable solubility behavior (Example 6).

A generic model is developed to treat the simultaneous processes of dissolution, reaction, mass transfer, nucleation

and growth occurring during reactive crystallization. The mass-transfer Damköhler number, nucleation number, and growth number determine how far the process path strays from the solubility surface. In addition, the dimensionless numbers compare the relative rates of the individual steps and provide insights for the resultant crystal size and crystallizer productivity.

The current approach can be extended in several ways. The crystallizer model is sufficiently generic and more details can be added such as the inclusion of gas-liquid reaction and the corresponding mass-transfer step. Effects like Ostwald ripening and agglomeration can be included in the crystal growth models. In that case, population balance equations will be incorporated explicitly into the model so as to track the particle-size distribution.

Acknowledgment

Acknowledgment is made to the donors of the Petroleum Research Fund, administered by the ACS, for support of this research.

Notation

a_S = surface area of dissolving solid reactant per unit suspension volume, m^2/m^3
a_T = surface area of growing crytals per unit suspension volume, m^2/m^3
C_i = concentration of species i in the liquid bulk, mol/m^3
F = volumetric flow rate, m^3/s
g = order of the crystal growth process (Eq. 12)
k_1, k_2 = first- and second-order reaction rate constants
k_g = crystal growth rate constant (Eq. 12), $(m/s)/(mol/m^3)^g$
k_n = nucleation rate constant (Eq. 11), no./$[m^3 s(mol/m^3)^n]$
k_s = solid-liquid mass-transfer coefficient, m/s
k_v = volumetric shape factor
K = reaction equilibrium constant
L_0 = size of nuclei, μm
n = order of nucleation rate (Eq. 11)
$n(L)$ = population density distribution of crystals, no./m^4
r = mean radius of reactant solid particles in the crystallizer, m
V = suspension volume, m^3
$w(L)$ = weight fraction distribution of crystals, m^{-1}
W = molar rate of addition of solid reactant, mol/s

Greek letters

ΔC = supersaturation, mol/m^3
Φ = molar reaction rate, mol/s
ρ_m = molar density of crystals, mol/m^3
τ = residence time of liquid in the crystallizer, s

Subscripts and superscripts

$*$ = at saturation conditions
i = pertaining to species i
$f, 0$ = pertaining to inlet (feed) conditions
s = pertaining to the liquid-crystal interface

Literature Cited

Berry, D. A., and K. M. Ng, "Synthesis of Reactive Crystallization Processes," *AIChE J.*, **43**, 1737 (1997).
Cisternas, L. A., and D. F. Rudd, "Process Design for Fractional Crystallization from Solution," *Ind. Eng. Chem. Res.*, **32**, 1993 (1993).
Cisternas, L. A., and R. E. Swaney, "Separation System Synthesis for Fractional Crystallization from Solution Using a Network Flow Model," *Ind. Eng. Chem. Res.*, **37**, 2761 (1998).
Dye, R. S., and K. M. Ng, "Fractional Crystallization: Design Alternatives and Tradeoffs," *AIChE J.*, **41**, 2427 (1995).
Franck, R., R. David, J. Villermaux, and J. P. Klein, "A Chemical Engineering Approach to Salicylic Acid Precipitation: Modeling of Batch Kinetics and Application to Continuous Operation," *Chem. Eng. Sci.*, **43**, 69 (1988).
Franke, J., and A. Mersmann, "The Influence of Operating Conditions on the Precipitation Process," *Chem. Eng. Sci.*, **50**, 1737 (1994).
Garside, J., and N. S. Tavare, "Crystallization as Chemical Reaction Engineering," *Inst. Chem. Eng. Symp. Ser.*, No. 87 (ISCRE 8), 767 (1984).
Kelkar, V. V., and K. M. Ng, "Screening Procedure for Synthesizing Isothermal Multiphase Reactors," *AIChE J.*, **44**, 1563 (1998).
Matsuoka, M., and J. Garside, "The Significance of Mass and Heat Transfer During Crystal Growth from Solutions and Melts," *J. Cryst. Growth*, **129**, 385 (1993).
Mersmann, A., and M. Kind, "Chemical Engineering Aspects of Precipitation from Solution," *Chem. Eng. Technol.*, **11**, 264 (1988).
Mullin, J. W., *Crystallization*, Butterworth-Heinemann, Oxford (1993).
Myerson, A. S., ed., *Handbook of Industrial Crystallization*, Butterworth-Heinemann, Boston (1993).
Nielsen, A. E., *Kinetics of Precipitation*, Pergamon, Oxford (1964).
Nyvlt, J., O. Söhnel, M. Matuchova, and M. Broul, *The Kinetics of Industrial Crystallization*, Elsevier, Amsterdam (1985).
Rajagopal, S., K. M. Ng, and J. M. Douglas, "Design of Solids Processes: Production of Potash," *Ind. Eng. Chem. Res.*, **27**, 2071 (1988).
Randolf, A. D., and M. A. Larson, *Theory of Particulate Processes*, 2nd ed., Academic, London (1988).
Rousseau, R. W., and F. P. O'Dell, "Separation of Multiple Solutes by Selective Nucleation," *Ind. Eng. Chem. Process Des. Dev.*, **19**, 603 (1980).
Söhnel, O., and J. Garside, *Precipitation: Basic Principles and Industrial Application*, Butterworth-Heinemann, Oxford (1992).
Tavare, N. S., *Industrial Crystallization: Process Simulation, Analysis and Design*, Plenum, New York (1995).
Tavare, N. S., and J. Garside, "Simulation of Reactive Precipitation in a Semi-batch Crysallizer," *Trans. Inst. Chem. Eng.*, **68**, 116 (1990).
Wachi, S., and A. G. Jones, "Mass Transfer with Chemical Reaction and Precipitation," *Chem. Eng. Sci.*, **46**, 1027 (1991).

Manuscript received July 29, 1998, and revision received Oct. 20, 1998.